Peer-Reviewed Technical Communication

Coherent Multipath Direction-of-Arrival Resolution Using Compressed Sensing

Anup Das, William S. Hodgkiss, *Member, IEEE*, and Peter Gerstoft, *Member, IEEE*

***Abstract*—For a sound field observed on a sensor array, performance of conventional high-resolution adaptive beamformers is affected dramatically in the presence of coherent multipath signals, but the directions-of-arrival (DOAs) and power levels of these arrivals can be resolved with compressed sensing (CS). When the number of multipath signals is sufficiently small, a CS approach can be used by formulating the problem as a sparse signal recovery problem. CS overcomes the difficulty of resolving coherent arrivals at an array by directly processing the sensor outputs without first estimating a sensor covariance matrix. CS is compared to the adaptive minimum-variance-distortionless-response (MVDR) spatial processor with spatial smoothing. Though spatial smoothing produces improved results by preprocessing the sensor array covariance matrix to decorrelate the coherent multipath components, it reduces the effective aperture of the array and hence reduces the resolution. An empirical study with a uniform linear array (ULA) demonstrates that CS outperforms MVDR beamformer with spatial smoothing in terms of spatial resolution and bias and variance of DOA and power estimates. Analysis of the shallow-water HF97 ocean acoustic experimental data shows that CS is able to recover the DOAs and power levels of the multipath signals with superior resolution compared to MVDR with spatial smoothing.**

***Index Terms*—Adaptive filter, beamforming, coherence, compressed sensing (CS), direction of arrival (DOA), multipath, sparse Bayesian learning (SBL), spatial smoothing.**

I. Introduction

The theory of compressed sensing (CS) has received growing attention due to its remarkable ability to reconstruct a sparse or compressible signal represented by an overcomplete set of basis functions from the observations or measurements with high probability [1]–[4]. CS has been applied successfully in medical imaging [5], [6], channel estimation [7], [8], radar imaging [9], [10], image processing [11], [12], audio processing [13], [14], geophysics and remote sensing [15]–[17], broadband underwater acoustic source localization [18], control systems [19], and pattern recognition and machine learning [20], [21], to name a few.

Among the applications of CS, estimating the directions-of-arrival (DOAs) of multiple signals using an array of sensors is of particular interest because if the number of signals is sufficiently small, we can represent the problem of estimating the DOAs as a sparse signal recovery problem in which the theory of CS is directly applicable. For the single snapshot case, matching pursuit methods [22]–[24], the basis pursuit method [25], [26], the iterative reweighted l_1 method [27], iterative reweighted l_2 methods [28], [29], and Bayesian methods [30]–[33] can be used to estimate the DOAs of multiple signals. For the multiple snapshot case, matching pursuit methods [34]–[36], basis pursuit methods [26], [35]–[37], the iterative reweighted l_1 method [38], the iterative reweighted l_2 method [35], and Bayesian methods [39], [40] can be used to solve the problem of estimating DOAs using CS theory.

The DOA estimation application of CS theory has been investigated in multiple efforts. This particular application of CS theory is especially attractive due to its higher resolution, robustness to noise, and good performance with a limited number of snapshots. Malioutov *et al.* [41] use the l_1-norm penalty for DOA estimation of multiple signals. Hyder and Mahata [42] use the l_0-norm penalty to enforce sparsity in the spatial domain to identify the DOAs of signals. In [40], Bayesian compressive sensing strategies based on the sparse Bayesian learning principle [30] have been utilized for estimating the DOAs. Tan and Nehorai [43] use coprime arrays and matching pursuit methods to locate the DOAs of signals. A greedy block coordinate descent algorithm exploiting spatial sparsity also has been used in [44] for the DOA estimation of multiple signals.

The most interesting observation in the aforementioned methods is that CS estimates the DOAs by directly processing the sensor outputs without first estimating a sensor covariance matrix. This important observation motivates the application of CS in estimating the DOAs of coherent multipath signals of a source (i.e., the multiple propagation paths from a single source have a deterministic relationship, thus in the absence of noise, the multipath arrivals will have a constant phase difference across snapshots). Coherent multipath propagation can be present in radar and sonar environments [45], deliberately induced coherent interferences by smart jammers [46], and cellular communication systems [47], [48].

The performance of CS in resolving the DOAs of coherent multipath signals is in contrast to that of conventional high-resolution adaptive spatial processors whose performance degrades dramatically when estimating the DOAs and power levels of signals that are coherent. In the minimum-variance-distortionless-response (MVDR) adaptive beamformer, the sensor outputs are combined by a weight vector such that the desired signal can pass with minimum distortion, while rejecting other interfering signals [49, Ch. 6, 7, and 9]. But in the presence of coherent multipath propagation, the MVDR beamformer not only fails to form deep nulls in the direction of coherent interferences, but also the desired signal in a particular direction can be partially or fully canceled in the output of the beamformer. To overcome the difficulty in estimating DOAs and power levels in a multipath scenario for a uniform linear array (ULA), the forward–backward spatial smoothing (FBSS) technique was proposed [50]–[52]. FBSS progressively decorrelates the multipath components at a rate that depends on the spacing and arrival directions

Manuscript received September 9, 2015; revised February 21, 2016 and April 25, 2016; accepted May 31, 2016. Date of publication July 29, 2016; date of current version April 12, 2017. This work was supported by the U.S. Office of Naval Research under Grant N00014-14-1-0439.

Associate Editor: W. Xu.

A. Das is with the Department of Electrical and Computer Engineering, University of California, San Diego, La Jolla, CA 92093 USA (e-mail: a1das@eng.ucsd.edu).

W. S. Hodgkiss and P. Gerstoft are with the Marine Physical Laboratory, Scripps Institution of Oceanography, University of California, San Diego, La Jolla, CA 92093 USA (e-mail: whodgkiss@ucsd.edu; pgerstoft@ucsd.edu).

Digital Object Identifier 10.1109/JOE.2016.2576198

of the coherent signals, thus providing less distortion in the coherent signal direction estimates and more rejection of them in the adaptive beamformer output. However, FBSS reduces the effective aperture of the sensor array, essentially reducing the resolution that would have been achieved in an incoherent scenario where no spatial smoothing is necessary and the processing makes use of the full aperture of the array.

Our objective in this paper is to experimentally demonstrate the recovery performance of the DOAs using CS and compare it with the MVDR beamformer with FBSS. For our CS-based simulations and experimental data analysis, we use the sparse Bayesian learning based relevance vector machine (SBL-RVM) algorithm for multiple snapshots or multiple measurement vectors (MMVs) [39] which was originally proposed for the single snapshot or single measurement vector (SMV) case [30], [53]. Our findings are as follows.

1) CS can resolve successfully the DOAs of coherent multipath signals since it processes the data directly without first estimating the sensor covariance matrix. This is in contrast to the MVDR beamformer whose performance is affected dramatically due to coherent multipath propagation.
2) CS is able to recover the DOAs and power levels of the multipath signals with higher resolution than MVDR with spatial smoothing when multiple snapshots are processed simultaneously.

The rest of the paper is organized as follows. In Section II, we describe the signal model and assumptions made on the statistics of signal and noise. In Section III, we formulate the multipath DOA estimation problem as a sparse signal recovery problem and briefly describe how it can be solved by using the SBL-RVM algorithm. In Section IV, extensive simulation study compares and contrasts MVDR with FBSS and SBL-RVM in resolving multipath signals with specific importance given to the results for bias and variance of the DOAs and power estimates of the multipath signals. In Section V, we demonstrate the high-resolution capability of SBL-RVM for estimating the DOAs and power levels of the multipath signals with data from the shallow-water HF97 ocean acoustic experiment. Last, we draw conclusions in Section VI.

II. Signal Model and Assumptions

We consider a ULA consisting of N identical sensors and receiving far-field plane wave signals from K multipath signals generated from a single source, i.e., there are K multipath signals in total including the source. We assume that the N sensors are located on the z-axis with uniform spacing equal to d and the center of the array is located at the origin of the coordinate system. Hence, the locations of the sensors along the z-axis are

$$z_n = \left(n - \frac{N-1}{2}\right) d, \quad n = 0, 1, \dots, N-1. \tag{1}$$

An angular spread $[0^\circ, 180^\circ]$ is also assumed with $\theta = 0^\circ$ denoting the positive z-axis direction. Hence, $\theta = 0^\circ$ and $\theta = 180^\circ$ correspond to the endfire directions and $\theta = 90^\circ$ corresponds to the broadside direction. We assume that we have preprocessed the sensor array data by taking fast Fourier transforms (FFTs) and hence the source signal and its multipath components are narrowband. Let λ denote the wavelength corresponding to the frequency of the source. These K multipath signals arrive at the array from directions $\theta_1, \theta_2, \dots, \theta_K$. At any instant j, these K signals $x_{1j}, x_{2j}, \dots, x_{Kj}$ are complex multiples of one of them at $z = 0$—say, the first—and hence

$$x_{kj} = c_k x_{1j}, \quad k = 1, 2, \dots, K \tag{2}$$

where c_k represents the complex attenuation of the kth signal with respect to the first signal x_{1j} and $c_1 = 1$. Using complex signal representation, the measurement at the array at the jth instant can be represented by

$$\mathbf{t}_{\cdot j} = \mathbf{A}\mathbf{x}_{\cdot j} + \mathbf{n}_{\cdot j} \tag{3}$$

where $\mathbf{t}_{\cdot j} \triangleq [t_{1j}, t_{2j}, \dots, t_{Nj}]^T$ is the $N \times 1$ array output data vector and

$$\mathbf{x}_{\cdot j} = [x_{1j}, x_{2j}, \dots, x_{Kj}]^T \tag{4}$$

$$\mathbf{n}_{\cdot j} = [n_{1j}, n_{2j}, \dots, n_{Nj}]^T \tag{5}$$

and

$$\mathbf{A} = [\mathbf{a}(\theta_1), \mathbf{a}(\theta_2), \dots, \mathbf{a}(\theta_K)]. \tag{6}$$

In (6), $\mathbf{a}(\theta_k)$ represents the direction vector associated with the kth multipath and given by

$$\mathbf{a}(\theta_k) = \frac{1}{\sqrt{N}} \left[e^{-j\frac{N-1}{2}\psi_k}, e^{-j\frac{N-3}{2}\psi_k}, \dots, e^{j\frac{N-1}{2}\psi_k} \right]^T \tag{7}$$

where $\psi_k = 2\pi (d)/(\lambda) \cos\theta_k$ and j is the square root of minus one. Here $(\cdot)^T$ denotes the transpose. Note that the direction vectors are l_2 normalized, i.e., $\mathbf{a}^H(\theta_k)\mathbf{a}(\theta_k) = 1$ for $k = 1, 2, \dots, K$ where $(\cdot)^H$ denotes the complex conjugate transpose. The $N \times 1$ vector $\mathbf{n}_{\cdot j}$ is the additive noise at the array at the jth instant.

After preprocessing the sensor array data with FFTs, the source signal [and hence its multipath components by (2)] is assumed to be a zero-mean, stationary complex Gaussian random process [54]. Furthermore, the source (and hence its multipath components) and the additive noise are assumed to be independent of each other. Each noise vector also is assumed to be a zero-mean, stationary complex Gaussian random process. Furthermore, it is assumed that the noises are uncorrelated sensor to sensor and across measurements with common variance σ^2.

III. Coherent Multipath DOA Estimation Using the CS Method

To cast the DOA estimation problem in a CS framework, the estimation of the multipath DOAs must be formulated as a problem of sparse signal recovery in an overcomplete matrix. We first describe the CS method and then show its performance in an example highlighting the impact of coherence between multipath signals.

A. CS Method

We discretize the angular spread [0°, 180°] of the ULA to result in M steering vectors having the same formulation as the direction vectors given in (7). We construct the $N \times M$ matrix $\mathbf{\Phi}$ which contains the M steering vectors as its columns. Note that matrix $\mathbf{A}$ in (6) contains the direction vectors of the multipath signals whereas matrix $\mathbf{\Phi}$ contains the steering vectors of the DOAs where a multipath may or may not be present. We construct the $M \times L$ matrix $\mathbf{W}$ where any particular row contains the complex amplitudes of a multipath corresponding to the steering vector in $\mathbf{\Phi}$ if a multipath is present in that steering direction or zero otherwise. We make the further assumption that a very few number of multipath signals are present, i.e., $\mathbf{W}$ is row sparse. We represent the array output vectors $\mathbf{t}_{\cdot j}$ as the columns of a matrix $\mathbf{T}$ and the noise vectors $\mathbf{n}_{\cdot j}$ as the columns of a matrix $\mathcal{E}$. Assuming L snapshots, the set of equations in (3), where $j = 1, 2, \dots, L$, can be represented equivalently as

$$\mathbf{T} = \mathbf{\Phi}\mathbf{W} + \mathcal{E}. \tag{8}$$

We note that in (8), the objective is to recover the row sparse matrix $\mathbf{W}$ given the observation matrix $\mathbf{T}$ and the overcomplete matrix $\mathbf{\Phi}$, giving rise to a noisy sparse signal recovery problem with MMVs. Several deterministic CS methods [35]–[37], [55]–[57] have been proposed in literature which can be used to estimate the DOAs of the multipath signals. But a few major issues are involved in such deterministic methods.

1) A good estimation of the regularization parameters (see the references for details) balancing sparsity and error is a difficult task in practice. Often computationally expensive cross-validation (CV) methods [58]–[60] or Markov chain Monte Carlo (MCMC) methods [61], [62] are employed to tackle this problem. However, since these methods are not based on a generalized principle, efficient estimation of the regularization parameters is difficult. A large regularization parameter may give a more sparse and less representative solution of the data resulting in the underestimation of the number of multipath signals whereas a small regularization parameter may result in a less sparse solution giving a good fitting to the noisy data resulting in the overestimation of the number of multipath signals.
2) Since the deterministic methods use a fixed prior for inducing sparsity (see the references for details), a good selection of the fixed prior also is a difficult task in practice. If a moderately sparse prior is chosen as used in basis pursuit methods [35]–[37], then the solution is convergent globally, but the solution may not be sufficiently sparse, whereas, if a highly sparse prior is chosen as used in the iterative reweighted l_2 method [35], then the solution may achieve the desired sparseness, but there will be several local optima to which the solution may converge.

An algorithm was proposed in [39] for solving the simultaneous sparse signal recovery problem and is known as the SBL-RVM algorithm. SBL-RVM overcomes the difficulties of estimating the regularization parameters and the choice of the fixed prior. This is a fully automated relevance determination algorithm based on the Bayesian evidence maximization framework originally introduced by MacKay [63]. The distinctive features of this algorithm are as follows.

1) The use of an empirical prior dependent on a set of unknown hyperparameters which are estimated from the data. This increases the chances of SBL-RVM converging to the global optimum without getting stuck at one of the local minima.
2) The parameters (σ^2 and $\boldsymbol{\gamma}$) which control the balance between sparsity and modeling error in SBL-RVM also are estimated from the data.

We use the SBL-RVM algorithm proposed in [39] to solve (8). In [39], the algorithm was derived for the real data case. Here we extend the real version of SBL-RVM to the complex data case. This can be done with slight modifications. We describe the major steps involved in this algorithm and refer the reader to [39] for the theoretical details.

We assume $p\left(\mathbf{T}|\mathbf{W};\sigma^2\right)$ to be complex Gaussian [54] with noise variance σ^2 which is unknown. Thus, for each $\mathbf{t}_{\cdot j}, \mathbf{w}_{\cdot j}$ pair, we have the likelihood of the array output as

$$p\left(\mathbf{t}_{\cdot j}|\mathbf{w}_{\cdot j};\sigma^2\right) = \left(\pi\sigma^2\right)^{-N} \exp\left(-\frac{1}{\sigma^2}\|\mathbf{t}_{\cdot j} - \mathbf{\Phi}\mathbf{w}_{\cdot j}\|_2^2\right) \quad (9)$$

and hence

$$p\left(\mathbf{T}|\mathbf{W};\sigma^2\right) = \prod_{j=1}^{L} p\left(\mathbf{t}_{\cdot j}|\mathbf{w}_{\cdot j};\sigma^2\right). \quad (10)$$

We assign to the ith row of $\mathbf{W}$ an L-dimensional complex Gaussian prior

$$p\left(\mathbf{w}_{i\cdot};\gamma_i\right) \triangleq \mathcal{CN}\left(0;\gamma_i\mathbf{I}\right) \quad (11)$$

where γ_i is an unknown variance parameter. By combining all the row priors, we arrive at the full weight prior given by

$$p\left(\mathbf{W};\boldsymbol{\gamma}\right) = \prod_{i=1}^{M} p\left(\mathbf{w}_{i\cdot};\gamma_i\right) \quad (12)$$

whose form is parameterized by the hyperparameter vector $\boldsymbol{\gamma} = \left[\gamma_1,\gamma_2,\ldots,\gamma_M\right]^T \in \mathbb{R}_+^M$. Combining likelihood and prior, the posterior density of the jth column of $\mathbf{W}$ then becomes

$$p(\mathbf{w}_{\cdot j}|\mathbf{t}_{\cdot j};\boldsymbol{\gamma},\sigma^2) = \frac{p(\mathbf{w}_{\cdot j},\mathbf{t}_{\cdot j};\boldsymbol{\gamma},\sigma^2)}{\int p(\mathbf{w}_{\cdot j},\mathbf{t}_{\cdot j};\boldsymbol{\gamma},\sigma^2)d\mathbf{w}_{\cdot j}} = \mathcal{CN}(\boldsymbol{\mu}_{\cdot j},\mathbf{\Sigma}) \quad (13)$$

with covariance and mean given, respectively, by

$$\begin{aligned}\mathbf{\Sigma} &= \mathbf{\Gamma} - \mathbf{\Gamma}\mathbf{\Phi}^H\mathbf{\Sigma}_t^{-1}\mathbf{\Phi}\mathbf{\Gamma} \quad \forall j = 1,\ldots,L\\ \mathcal{M} &= [\boldsymbol{\mu}_{\cdot 1},\ldots,\boldsymbol{\mu}_{\cdot L}] = \mathbf{\Gamma}\mathbf{\Phi}^H\mathbf{\Sigma}_t^{-1}\mathbf{T}\end{aligned} \quad (14)$$

where $\mathbf{\Gamma} \triangleq \operatorname{diag}(\boldsymbol{\gamma})$ and $\mathbf{\Sigma}_t \triangleq \sigma^2\mathbf{I} + \mathbf{\Phi}\mathbf{\Gamma}\mathbf{\Phi}^H$. Hence, row sparsity is achieved whenever a γ_i is equal to zero ensuring that the posterior mean of the ith row, $\boldsymbol{\mu}_{i\cdot}$, is zero as desired.

We then adopt an empirical Bayesian strategy treating the unknown weights $\mathbf{W}$ as nuisance parameters and integrate them out of the integrand in (15). This results in the following marginal likelihood which is a function of $\boldsymbol{\gamma}$ and σ^2:

$$\begin{aligned}\mathcal{L}\left(\boldsymbol{\gamma},\sigma^2\right) &\triangleq -\log\int p\left(\mathbf{T}|\mathbf{W};\sigma^2\right)p\left(\mathbf{W};\boldsymbol{\gamma}\right)d\mathbf{W}\\ &= -\log p\left(\mathbf{T};\boldsymbol{\gamma}\right) \propto L\log|\mathbf{\Sigma}_t| + \sum_{j=1}^{L}\mathbf{t}_{\cdot j}^H\mathbf{\Sigma}_t^{-1}\mathbf{t}_{\cdot j}.\end{aligned} \quad (15)$$

The factor $-\log(\cdot)$ is added to simplify calculations. The marginal likelihood in (15) also is referred to as the evidence for the parameters σ^2 and $\boldsymbol{\gamma}$ in [63] and its maximization is known as the evidence maximization. The marginal likelihood in (15) can be maximized directly by taking derivatives with respect to the parameters γ_i and σ^2 [39]. We, however, use the expectation–maximization (EM) algorithm to maximize (15) by treating the weights $\mathbf{W}$ as the hidden variables and maximize $E_{\mathbf{W}|\mathbf{T};\boldsymbol{\gamma},\sigma^2}[\log p(\mathbf{T}|\mathbf{W};\sigma^2)p(\mathbf{W};\boldsymbol{\gamma})]$. For $\boldsymbol{\gamma}$, ignoring the terms in the logarithm independent thereof, we equivalently maximize

$$E_{\mathbf{W}|\mathbf{T};\boldsymbol{\gamma},\sigma^2}\left[\log p\left(\mathbf{W};\boldsymbol{\gamma}\right)\right] \quad (16)$$

which through differentiation gives the update equations for γ_i as [39]

$$\gamma_i^{(\text{new})} = \frac{1}{L}\|\boldsymbol{\mu}_{i\cdot}\|_2^2 + \mathbf{\Sigma}_{ii} \quad \forall i = 1,\ldots,M. \quad (17)$$

Following the corresponding procedure for the noise level σ^2, we equivalently maximize

$$E_{\mathbf{W}|\mathbf{T};\boldsymbol{\gamma},\sigma^2}\left[\log p\left(\mathbf{T}|\mathbf{W};\sigma^2\right)\right] \quad (18)$$

which gives [64]

$$\left(\sigma^2\right)^{(\text{new})} = \frac{\frac{1}{L}\|\mathbf{T} - \mathbf{\Phi}\mathcal{M}\|_{\mathcal{F}}^2 + \left(\sigma^2\right)^{(\text{old})}\left(M - \sum_{i=1}^{M}\frac{\mathbf{\Sigma}_{ii}}{\gamma_i}\right)}{N}. \quad (19)$$

Equations (14), (17), and (19) are the iterative equations for the SBL-RVM. The algorithm is summarized in Table I. The EM procedure provided better performance in recovery of the

TABLE I
SUMMARY OF THE SBL-RVM ALGORITHM

Given the observation data $\mathbf{T}$ and the overcomplete matrix $\mathbf{\Phi}$ containing the steering vectors, SBL-RVM can be summarized as follows.

(i) Initialize γ and σ^2.

(ii) Compute the posterior moments $\mathbf{\Sigma}$ and $\mathcal{M}$ using (14).

(iii) Update γ using (17) and σ^2 using (19).

(iv) Iterate (ii) and (iii) until convergence. Declare the algorithm to be converged when the change in γ is less than some predefined threshold.

(v) After convergence, the value of $\mathcal{M}$ is the estimate of the desired weight matrix $\mathbf{W}$. SBL-RVM forces the entries in the rows of $\mathbf{W}$ to be zero in which a multipath component is not present and consequently choosing the most relevant columns in the matrix $\mathbf{\Phi}$ which denote the DOAs of the multipath signals.

weights $\mathbf{W}$ than direct differentiation of (15) for our multipath DOA resolution application. For an analysis of the complexity and convergence properties of the SBL-RVM algorithm, see [39].

SBL-RVM directly performs processing of the data $\mathbf{T}$ without any sensor covariance matrix estimation and hence overcomes the difficulty of coherent arrivals in the case of multipath signals which is the primary source of performance degradation for adaptive beamformers such as MVDR. In [65], it was shown empirically that SBL-RVM is independent of correlation among the signals. This feature of SBL-RVM makes it highly attractive for use in applications that involve estimating DOAs and power levels of multipath signals. Though we have considered a linear array for our simulations (Section IV) and experimental data analysis (Section V), SBL-RVM is applicable to arrays of arbitrary geometry.

SBL-RVM can estimate the DOAs of the multipath signals with a single snapshot. Performance of CS in the DOA estimation problem with a single snapshot already has been evaluated [55]–[57]. In contrast, DOA estimation in MVDR with FBSS with a single snapshot, in general, is difficult. This feature of CS makes it very attractive in applications where a limited number of snapshots are available. Performance of SBL-RVM improves as more snapshots are available. CS methods for the multiple snapshot case have better performance than those of the single snapshot case since considering multiple snapshots altogether significantly decreases the error in DOA estimates which is due to the effect of noise (see the references for the CS methods for the multiple snapshot case for more details).

The most salient feature of CS is its higher resolution as compared to MVDR with FBSS. Theoretical results for the probability of resolution of CS have been discussed in [55] whereas the analysis of the same for the MVDR beamformer is done in [66]. Our analysis, however, is empirical (see Section IV). For our analysis, we define a resolution criterion as done in [67]. Let θ_1 and θ_2 denote the true angles of arrivals of two multipath signals and let $\theta' = (\theta_1 + \theta_2)/2$ denote the mid-angle between them. Let $\hat{P}(\theta_1)$, $\hat{P}(\theta_2)$, and $\hat{P}(\theta')$ denote the estimated power levels at the angles θ_1, θ_2, and θ' respectively. We define a resolution event as

$$\xi(\theta_1, \theta_2) \triangleq \frac{1}{2}\left\{\hat{P}(\theta_1) + \hat{P}(\theta_2)\right\} - \hat{P}(\theta'). \tag{20}$$

We say that two multipath signals are resolvable if the average of the power levels at the angles of arrivals of the two multipath signals is greater than the power level at the mid-angle and irresolvable otherwise. Hence, the probability of resolution can be written as

$$P_{\text{res}} = \Pr\{\xi > 0\}. \tag{21}$$

SBL-RVM suffers from grid bias due to discretization of angular spread. If the discretization of the angular spread is too coarse, then grid bias will be present in SBL-RVM DOA estimation due to the fact that the true scenario DOAs will not be exactly aligned with the steering vectors in the overcomplete dictionary $\mathbf{\Phi}$. This is known as basis mismatch in CS literature. As a result, the weight matrix $\mathbf{W}$ will not be sparse in the assumed basis $\mathbf{\Phi}$, rather it is sparse in the true underlying basis $\mathbf{\Phi}'$. The effect of grid bias may result in large error in the recovery of sparse $\mathbf{W}$. The effect of grid bias or basis mismatch on the recovery performance of CS already has been studied in [68] and [69]. At the other extreme, if the discretization of the angular spread is too fine, then adjacent steering vectors in the overcomplete dictionary $\mathbf{\Phi}$ will be heavily correlated and the spatial spectral power will spread over the adjacent steering vectors which may result in grid bias [70]. The grid bias is expected to appear in any CS based DOA estimation approach that involves a discretization of the continuous angular domain.

Grid refinement methods [41], [70], [71] have been proposed in the CS literature to mitigate the effect of grid bias. To get rid of the problems due to grid bias altogether, off-the-grid CS methods [72], [73] also have been proposed. We, however, restrict ourselves to on-grid CS and assume that the DOAs are aligned with the steering vectors for our simulations (Section IV) and experimental data analysis (Section V).

SBL-RVM suffers from inherent bias [71] due to the inaccuracy in the estimation of the noise level σ^2 and the variance parameter γ_i. The noise parameter σ^2 and the variance parameter γ_i determine the tradeoff between sparsity in the solution and fitting of the model to the noisy data [74]. Inaccuracy in the estimation of these two parameters may result in the overestimation or underestimation of the number of signals.

It is well known that CS underestimates the power levels due to the regularization parameter resulting in a large bias in the power estimates. SBL-RVM underestimates the power levels mainly due to the noise parameter σ^2 and the variance parameter γ_i both of which determine the balance bewteen sparsity and model fitting. Hence a least squares (LS) estimate of the power levels of the multipath signals can be obtained [35], [75]–[77] after the DOAs have been identified in SBL-RVM.

B. Demonstration of DOA and Power Level Estimation

As a demonstration of the high-resolution capability of SBL-RVM for estimating multipath DOAs and power levels, we give an example in Fig. 1. We consider three multipath signals of equal power impinging on an array of 12 sensors (i.e., $N = 12$) with half-wavelength spacing between the array elements from directions $\theta_1 = 45^\circ$, $\theta_2 = 60^\circ$, and $\theta_3 = 67^\circ$. The power of the kth multipath is defined as $\sigma_s^2 \triangleq E[|x_{kj}|^2]$. In this example, the power of each multipath is taken to be -40 dB, i.e., $10\log_{10}(\sigma_s^2) = -40$. For each individual multipath at each sensor the input signal-to-noise ratio (SNR) is defined to be

$$\text{SNR} = 10\log_{10}\left(\frac{\sigma_s^2}{\sigma^2}\right) \tag{22}$$

where σ^2 is the variance of the ith sensor noise sequence defined as $\sigma^2 \triangleq E[|n_{ij}|^2]$. We take SNR $= 25$ dB in this example. We consider a total of 50 snapshots, i.e., $L = 50$. To plot the spatial power spectrum, a 0.2° discretization on the angular spread $[0^\circ, 180^\circ]$ is taken.

For SBL-RVM, we first estimated the spatial power spectrum and rejected all the peaks in the power spectrum whose power levels were more than 15 dB below the highest peak and then reestimated the power

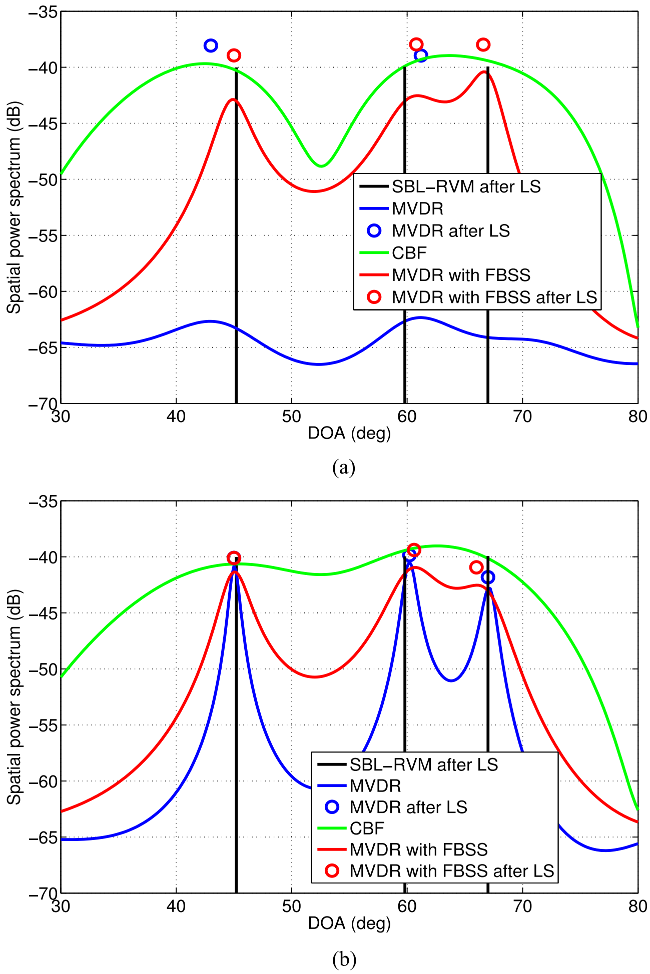

Fig. 1. Demonstration of estimating DOAs and power levels with SBL-RVM. Signal arrivals of equal power levels (−40 dB) at angles of $\theta_1 = 45^\circ, \theta_2 = 60^\circ$, and $\theta_3 = 67^\circ$ and SNR $= 25$ dB are considered. For comparison, we have included the DOA and power estimates for MVDR, MVDR with FBSS, and CBF. (a) Coherent signals (multipath signals). (b) Uncorrelated signals.

levels of the remaining peaks by using LS. The total number of these remaining peaks is selected as the total number of multipath signals in SBL-RVM.

For comparison, we also have included the results for the MVDR beamformer and the MVDR beamformer with FBSS. The estimated power $\hat{P}_{\text{SS}}(\theta)$ at the output of the filter for MVDR with FBSS, for a particular angle θ is [49, Ch. 6, 7, and 9].

$$\hat{P}_{\text{SS}}(\theta) = \frac{1}{\mathbf{a}^H(\theta)\,\widehat{\mathbf{R}}_{\text{SS}}^{-1}\,\mathbf{a}(\theta)} \tag{23}$$

where the smoothed array covariance matrix is estimated as

$$\widehat{\mathbf{R}}_{\text{SS}} = \frac{1}{2DL}\sum_{j=1}^{L}\sum_{g=1}^{D}\left[\mathbf{t}_{\cdot j_g}^{(N_0)}\left[\mathbf{t}_{\cdot j_g}^{(N_0)}\right]^H + \mathbf{J}\left[\mathbf{t}_{\cdot j_g}^{(N_0)}\right]^*\left[\mathbf{t}_{\cdot j_g}^{(N_0)}\right]^T\mathbf{J}\right]. \tag{24}$$

In FBSS, we divide the ULA of size N into uniformly overlapping forward and backward subarrays of size N_0 giving rise to $D\ (= N - N_0 + 1)$ forward subarrays and D backward subarrays. A subarray size of $N_0 = 9$ is considered for the FBSS case. In (24), $\mathbf{t}_{\cdot j_g}^{(N_0)}$ denotes the gth forward subarray at the jth instant, $\mathbf{J}$ denotes the $N_0 \times N_0$ exchange matrix, and $(\cdot)^*$ denotes the complex conjugate. Note that, in (23), the definition of $\mathbf{a}(\theta)$ is modified from (7) by substituting N_0 for N with θ corresponding to an arbitrary arrival angle. The DOAs of the K multipath signals are estimated as the DOAs corresponding to the K largest peaks in the spatial power spectrum given in (23). We define a peak as the point in the spatial power spectrum whose power level is greater than the power levels both at its left and right neighboring angles. Also note that to calculate the power for just the MVDR beamformer, we have to replace $\widehat{\mathbf{R}}_{\text{SS}}^{-1}$ in (23) with $\widehat{\mathbf{R}}^{-1}$ where $\widehat{\mathbf{R}}$ is the estimated array covariance matrix. Similar to SBL-RVM, an LS estimate of the power levels in MVDR with FBSS [78] is obtained since FBSS may not perfectly decorrelate the coherent multipath signals [49, Ch. 6, 7, and 9] and hence signals can be partially cancelled.

Last, for comparison, we also have shown in Fig. 1 the estimated power of the nonadaptive conventional beamformer (CBF). The CBF spatial power spectrum $\hat{P}_{\text{CBF}}$ is defined as [49, Ch. 2]

$$\hat{P}_{\text{CBF}}(\theta) = \mathbf{a}^H(\theta)\,\widehat{\mathbf{R}}\mathbf{a}(\theta) \tag{25}$$

where θ denotes an arbitrary arrival angle. Note that the CBF spectrum in (25) does not require spatial smoothing and hence the processing takes advantage of the entire array aperture. However, typically a spatial window function is used for sidelobe control. For the simulation shown in Fig. 1 and experimental data results shown later in Fig. 8, a Dolph–Chebyshev spatial window is used with a uniform sidelobe level of 28 dB below the mainlobe peak.

In Fig. 1(a), we note substantial signal cancellation with the MVDR beamformer in the unsmoothed case due to coherent multipath arrivals. Due to signal cancellation, not only do we obtain more inaccurate estimate of the DOAs than in the FBSS case, but we also are not able to resolve the closely spaced multipath signals at $\theta_2 = 60^\circ$ and $\theta_3 = 67^\circ$. The two DOAs estimated by MVDR were 43° and 61.2°. With FBSS, we obtain an estimate of the DOAs (45°, 60.8°, and 66.6°) and the power levels for all three arrivals in the MVDR beamformer. We also note that even though there is a difference in the DOA estimates in the unsmoothed and FBSS cases for the multipath signals at $\theta_1 = 45^\circ$ and $\theta_3 = 60^\circ$, the LS power estimates at each of these DOAs are very close to each other. We note that SBL-RVM overcomes the problem of coherent multipath arrivals and gives the most accurate estimates of DOAs (45.2°, 59.8°, and 67°) and power levels. Also, even though there is a difference in the DOA estimates in SBL-RVM and MVDR with FBSS for all three arrivals of the multipath signals, the LS power estimates are very close to each other. The low-resolution CBF was not able to resolve the three signals with DOA estimates at 42.4° and 63.6°. However, the overall spatial structure of the simulated field is indicated.

For comparison, we also have shown the estimated DOAs and power levels for SBL-RVM, MVDR and CBF in Fig. 1(b) when the signals are uncorrelated. Note that in this case, the MVDR beamformer is able to resolve the DOAs (the estimated DOAs are 45°, 60.2°, and 67°) of the three signals with good resolution and there is no signal cancellation. The estimated DOAs by SBL-RVM did not change indicating the robustness of SBL-RVM algorithm with respect to the correlation between the signals. As before, CBF could not resolve the signals with DOA estimates at 45.2° and 62.6°. Also note that there is no advantage of using MVDR with FBSS in the case of uncorrelated signals. These results are included to underscore that when using MVDR with FBSS there is a reduction in resolution.

Since the focus of the paper is on coherent multipath signals, we exclude the MVDR beamformer and low-resolution CBF from our

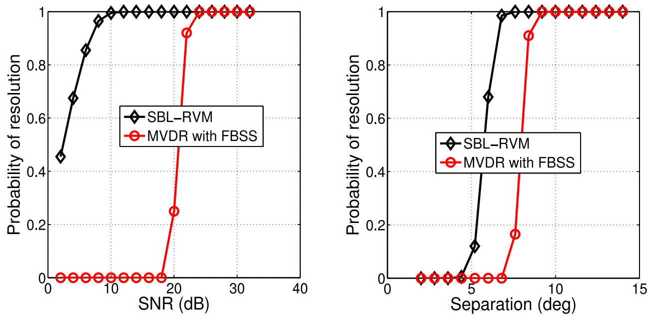

Fig. 2. Probability of resolution analysis for SBL-RVM and MVDR with FBSS. (a) Probability of resolution versus SNR for two multipath signals at 60° and 66°. (b) Probability of resolution versus separation between two multipath signals at SNR $= 4$ dB.

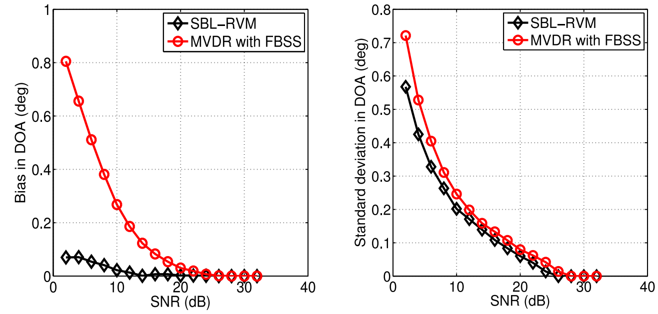

Fig. 3. Bias and standard deviation in DOA estimate versus SNR for SBL-RVM and MVDR with FBSS for the multipath at 60°. (a) Bias versus SNR. (b) Standard deviation versus SNR.

analysis in Section IV and only focus on SBL-RVM and MVDR with FBSS.

IV. Simulations

Before we proceed to the analysis of experimental data, we first evaluate the performance of SBL-RVM and MVDR with FBSS in simulation. In this section, we first carry out a probability of resolution analysis. Next, we provide an empirical analysis of bias and standard deviation in the DOA estimates of SBL-RVM and MVDR with FBSS. Last, an empirical analysis of bias and standard deviation in the power estimates (using LS) at the estimated DOAs (which may be biased) is provided.

For all the simulations, we consider a 12-element ULA with half-wavelength spacing between the array elements. A 0.2° discretization on the angular spread and $L = 50$ snapshots are assumed. For MVDR with FBSS, a subarray size of $N_0 = 9$ is used giving a degree of spatial smoothing $D = 4$.

A. Probability of Resolution Analysis of SBL-RVM and MVDR With FBSS

We next demonstrate the ability of SBL-RVM to resolve multipath signals with higher resolution as compared to MVDR with FBSS by using the probability of resolution criterion given in (20).

First, in Fig. 2(a), we calculate the probability of resolution in terms of the input SNR in 2-dB increments starting at 2 dB. For this we consider two multipath signals impinging on the ULA from DOAs 60° and 66° and the input SNR for each multipath at each sensor is assumed to be the same. For each input SNR, in total 200 trials are taken and the probability of resolution is calculated as the number of times an algorithm (SBL-RVM or MVDR with FBSS) is able to resolve the multipath signals using the criterion given in (20) divided by the total number of trials. We observe that SBL-RVM exhibits significantly higher resolution at low SNRs compared to MVDR with FBSS.

Next, in Fig. 2(b), we calculate the probability of resolution in terms of the separation between two multipath signals. For this we fix the DOA of one multipath at 60° and the second multipath is gradually separated from the first multipath with an increment of 0.8° starting from a DOA of 62°. The input SNR for each multipath at each sensor is equal and taken to be 4 dB. For each separation, in total 200 trials are taken and the probability of resolution is calculated as done in Fig. 2(a). We observe that the resolution of SBL-RVM is comparable to that of MVDR with FBSS. However, the significant advantage of SBL-RVM in terms of spatial resolution is very clear in Fig. 2(a).

B. Bias and Standard Deviation Analysis in DOA Estimates in SBL-RVM and MVDR With FBSS

First, we define the bias as $E[\hat{\theta}] - \theta$ and the standard deviation as $\sqrt{E[\hat{\theta} - E[\hat{\theta}]]^2}$. Here $\hat{\theta}$ denotes the estimated DOA of a particular multipath by SBL-RVM or MVDR with FBSS and θ denotes the true DOA of the multipath.

We now proceed to the bias and standard deviation analysis in the DOA estimates for SBL-RVM and MVDR with FBSS. We consider two multipath signals impinging on the ULA from DOAs 60° and 75° having equal input SNR. A separation of 15° is chosen such that both SBL-RVM and MVDR with FBSS are able to resolve the two multipath signals. For each input SNR, we consider in total 200 trials and calculate the bias and the standard deviation for the multipath at 60° for both methods. The bias is shown in Fig. 3(a) and the standard deviation is shown in Fig. 3(b). From the bias curve, we observe that on, an average, SBL-RVM has much better performance than MVDR with FBSS, whereas, from the standard deviation curve, we note that the variability in SBL-RVM and the variability in MVDR with FBSS are comparable to each other.

We then study the bias and standard deviation in the DOA estimates for SBL-RVM and MVDR with FBSS when multipath signals with unequal power levels are present. We consider three multipath signals impinging on the ULA from DOAs 45°, 60°, and 75°. Once again a separation of 15° is considered so that both methods are able to resolve the multipath signals. The input SNR for the multipath signals at 45° and 75° is kept equal and fixed at 8 dB. The power level for the multipath at 60° initially is taken to be equal to the power level of the other two multipath signals and then gradually decreased relative to the other two multipath signals in increments of 0.5 dB. In other words, the middle multipath is gradually buried in more noise keeping the power levels of the other two multipath signals fixed. For each relative decrease of the power level of the multipath at 60°, we take in total 200 trials and calculate the bias and the standard deviation for both methods. The bias is shown in Fig. 4(a) and the standard deviation is shown in Fig. 4(b). We observe from both curves that as the middle multipath power level is gradually lowered, performance of MVDR with FBSS gets progressively worse whereas SBL-RVM remains relatively stable showing the robustness of SBL-RVM in estimating the DOAs in the presence of multipath signals with unequal power levels.

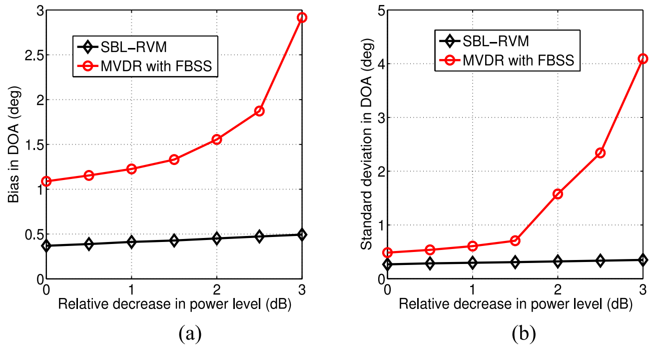

Fig. 4. Bias and standard deviation in DOA estimate versus relative decrease in power level for a middle multipath for SBL-RVM and MVDR with FBSS. (a) Bias versus relative decrease of power level for the multipath at 60°. (b) Standard deviation versus relative decrease of power level for the multipath at 60°.

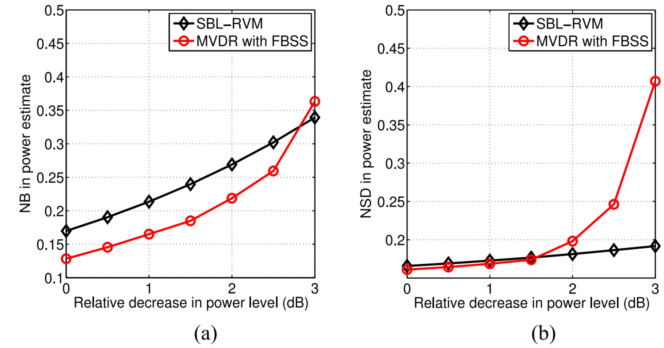

Fig. 6. Bias and standard deviation of the power estimate versus relative decrease of power level for a middle multipath for SBL-RVM and MVDR with FBSS. (a) Bias of the power estimate versus relative decrease of power level for the multipath at 60°. (b) Standard deviation of the power estimate versus relative decrease of power level for the multipath at 60°.

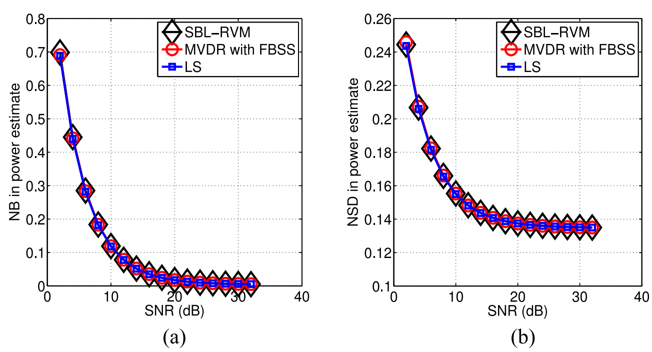

Fig. 5. Bias and standard deviation of the power estimate for SBL-RVM and MVDR with FBSS for the multipath at 60°. For comparison, also shown is the LS power estimate plot for the true DOA of 60°. (a) Bias of the power estimate versus SNR. (b) Standard deviation of the power estimate versus SNR.

C. Bias and Standard Deviation Analysis in Power Level Estimates in SBL-RVM and MVDR With FBSS

First, we define the normalized bias (NB) as $(E[\hat{P}(\hat{\theta})] - \sigma_s^2)/\sigma_s^2$ and the normalized standard deviation (NSD) as $\sqrt{(E[\hat{P}(\hat{\theta}) - E[\hat{P}(\hat{\theta})]]^2)/\sigma_s^4}$. Here $\hat{P}(\hat{\theta})$ denotes the estimated power level at the estimated DOA $\hat{\theta}$ of a particular multipath by SBL-RVM or MVDR with FBSS and σ_s^2 denotes the true power level of the multipath. The objective here is to study the bias and standard deviation of the estimated power level at the estimated DOA (which may or may not be biased) for a multipath for a method.

We now proceed to the analysis of NB and NSD in the power estimates for SBL-RVM and MVDR with FBSS. We consider two multipath signals impinging on the array from DOAs 60° and 75° so that both methods are able to resolve them. The input SNR for each multipath at each sensor is assumed to be equal. After estimating the DOAs for the multipath signals, we apply LS to reestimate the power levels. For each input SNR we consider a total of 200 trials and calculate the NB and the NSD in the power estimate for the multipath at 60°. The NB is shown in Fig. 5(a) and the NSD is shown in Fig. 5(b). In Fig. 5(a) and (b), we also have plotted the NB and the NSD curves for the LS estimate (denoted simply as LS in the plots) which is the NB and the NSD in the estimated power level of the true DOA (unbiased) of the multipath. From Fig. 5(a) and (b), we note that SBL-RVM, MVDR with FBSS, and LS produce almost identical curves for NB and NSD in the power estimate denoting that even if there is a difference in bias and standard deviation in the DOAs [see Fig. 3(a) and (b)] in SBL-RVM and MVDR with FBSS, the power levels for both of the methods estimated by LS are the same and also equal to the true DOA LS power estimate. Comparing Figs. 3(a) and 5(a), we observe that a bias of 1° or less is not enough to have a significant impact on the estimate of the power levels. Rather the NB and NSD in the power estimate in Fig. 5(a) and (b) can be attributed to the effect of noise.

We then study the NB and NSD in the power estimates for SBL-RVM and MVDR with FBSS when multipath signals with unequal power levels are present. We consider three multipath signals impinging on the ULA from DOAs 45°, 60°, and 75°. The input SNR for the multipath signals at 45° and 75° is kept equal and fixed at 8 dB. The power level for the multipath at 60° initially is taken to be equal to the power level of the other two multipath signals and then gradually decreased relative to the other two multipath signals in increments of 0.5 dB as done in Fig. 4. For each relative decrease of the power level of the multipath at 60°, we take a total of 200 trials and calculate the NB and NSD in the power estimate for both methods. The NB plot is shown in Fig. 6(a) and the NSD plot is shown in Fig. 6(b). From Fig. 6(a), we observe that as the middle multipath is buried under more noise, the NB for both SBL-RVM and MVDR with FBSS increases and also is comparable for both methods. Comparing Figs. 4(a) and 6(a), we note that, for SBL-RVM, though the bias in the DOA estimate remains almost the same, the NB in the power estimate increases, suggesting that the power estimate does not affect the DOA estimate. Comparing Figs. 4(b) and 6(b), we observe that the variability for both the DOA and power estimates in SBL-RVM is less than the variability for the same in MVDR with FBSS in the presence of multipath signals with unequal power levels.

V. The HF97 Ocean Acoustic Experiment

A. Overview of the Experiment

The HF97 experiment [79], [80] was carried out in shallow water off the coast of Point Loma, CA, USA, in October 1997. An overview of this experiment showing the source and receiver array (R/P FLIP) positions is shown in Fig. 7. The water depth was approximately 100 m and the source and the receiver were fixed to the bottom. The receiver consisted of a 64-element vertical linear array (VLA) and was deployed approximately 6 km away from the source. The interelement spacing of the VLA was $d = 0.1875$ m and the hydrophone elements of the

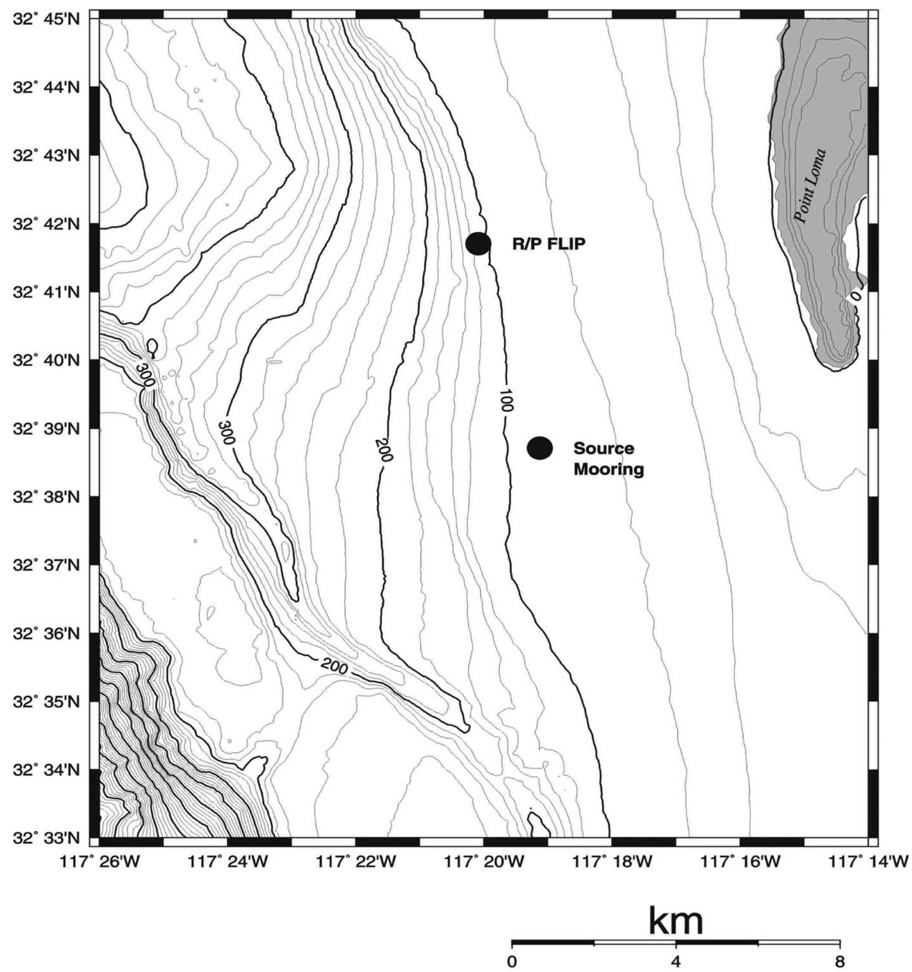

Fig. 7. Experiment overview showing the source mooring and receiving array locations in the HF97 experiment.

VLA were sampled at $f_s = 48$ kHz. The source transmitted several waveforms. Of interest here was the sinusoidal transmission at 1.9 kHz. The interelement spacing of the VLA is equivalent to 0.2375λ. We note that there is no spatial aliasing since at this frequency the interelement spacing is less than 0.5λ.

B. Data Processing

The start time of our data from the HF97 experiment is Julian Day 301 2210 UTC. First, we extract the 1.9-kHz tonal by using nonwindowed, nonoverlapping FFTs of length $2^{12} = 4096$. For the tonal, we process a total of 800 snapshots from the start time, divide the 800 snapshots into four blocks of 200 snapshots each, and resolve the multipath signals for each of the blocks of 200 snapshots using SBL-RVM and MVDR with FBSS. The 200 snapshots are approximately $(4096 \times 200) / (48000) = 17$ s duration and hence all 800 snapshots are approximately 68-s duration. In addition, the processing is repeated on the first 200 snapshots breaking them into four blocks of 50 snapshots each (approximately 4.25-s duration per block).

We use all 64 sensor elements of the VLA for processing. For MVDR with FBSS, a 47-element subarray is used for spatial smoothing. As before, a 0.2° discretization on the angular spread also is assumed.

C. Multipath DOA Resolution Results and Discussion

Here we demonstrate resolution of the multipath signals using SBL-RVM by processing 200 snapshots at a time for all 800 snapshots. Fig. 8 shows the resolved multipath signals for each of the 200 snapshots for the 1.9-kHz tonal for both SBL-RVM and MVDR with FBSS. For SBL-RVM, we first estimated the spatial power spectrum and rejected all the peaks in the power spectrum whose power levels were more than 15 dB below the highest peak and then reestimated the power levels of the remaining peaks by using LS as done before. The total number of these remaining peaks is selected as the total number of multipath signals. The choice of the value 15 dB was arbitrary.

There were no ground truth DOAs for this experiment. The nonadaptive CBF provides a reasonable (though not high-resolution) representation of the acoustic field observed by the array and hence was used as indicative of ground truth. Therefore, for comparison, we also have shown the estimated power of the nonadaptive CBF for all panels in Fig. 8. For estimating the spatial power spectrum of CBF we used a Dolph–Chebyshev spatial window whose sidelobe level was 28 dB below the mainlobe peak.

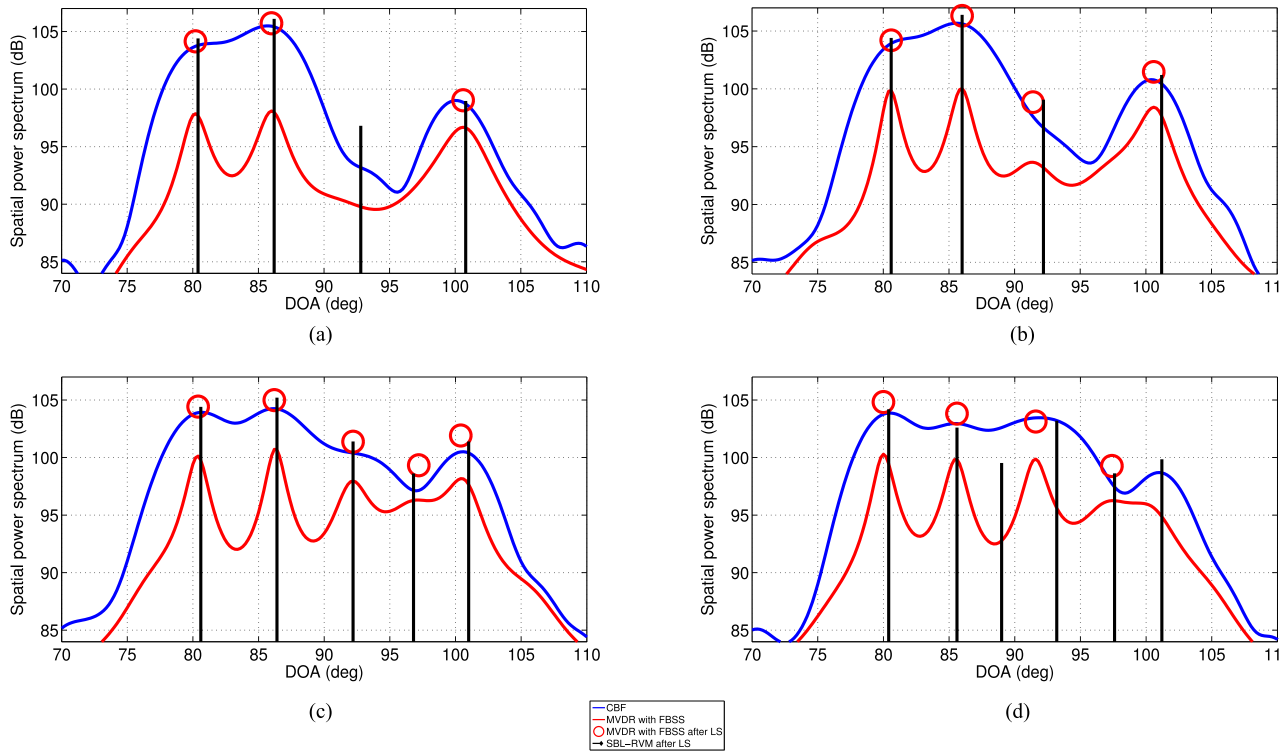

Fig. 8. Multipath resolution for the 1.9-kHz frequency in the HF97 experiment. Panels (a), (b), (c), and (d) correspond to the first, second, third, and fourth blocks of 200 snapshots (~17 s each), respectively.

Ray tracing results are shown in [79] using a CTD cast taken two hours after the data discussed here. These results suggest that a number of arrivals are expected approximately $\pm 10^\circ$ of broadside (broadside corresponds to 90° in Fig. 8). Similar ray tracing results are shown in [80] including the observed arrival angle versus travel time structure of the channel impulse response (obtained from processing LFM chirp waveforms that were transmitted simultaneously) at the same time the data discussed here was recorded. These also show a number of arrivals approximately $\pm 10^\circ$ of broadside. Thus, the DOA estimates of the multipath signals shown here are consistent with the propagation physics and modeling.

To check the validity of our multipath model in (2), we calculated the eigenvalue spectrum for each panel in Fig. 8. For each panel, the eigenvalue spectrum clearly showed one dominant eigenvalue (at least 15 dB higher than the others) indicating that the multipath signals are coherent and hence the coherent multipath propagation model in (2) is a good approximation.

From Fig. 8(a) and (d), we observe that MVDR with FBSS cannot resolve the DOAs of all of the multipath signals since it processes the data effectively using only 47 sensor elements and hence results in a reduced aperture implying reduced resolution. The subarray size 47 was chosen to obtain a good balance between resolution and degree of spatial smoothing. Other values for subarray size did not result in significant improvement in performance. The SBL-RVM algorithm, however, is able to identify the DOAs and power levels of the multipath signals with higher resolution than MVDR with FBSS and the results also are more consistent with the CBF spatial power spectrum than that of MVDR with FBSS in Fig. 8(a) and (d). In Fig. 8(a), we observe that SBL-RVM finds a multipath at 92.8° which is consistent with the CBF spectrum whereas MVDR with FBSS fails to form a peak. In Fig. 8(d), SBL-RVM finds two multipath signals at 89° and 93.2° and these results also are consistent with the unusually broadened spectrum by CBF near those angles (note that those angles are around broadside), but MVDR with FBSS is not able to resolve the DOAs of those multipath signals. Furthermore, in Fig. 8(d), SBL-RVM finds a multipath at 101.2° which is consistent with the CBF spectrum, but MVDR with FBSS fails to resolve it due to reduced effective array aperture and hence reduced resolution. The rest of the angles estimated by SBL-RVM and MVDR with FBSS were consistent with each other and also were consistent with the nonadaptive CBF.

Since one of the features of SBL-RVM is its capability to resolve the DOAs of multipath signals with a very few number of snapshots, we divided the first 200 snapshots corresponding to Fig. 8(a) into four consecutive blocks of 50 snapshots and estimated the DOAs using CBF, MVDR with FBSS and SBL-RVM. Note that in this case, the number of snapshots used in each block is just slightly larger than the subarray size (47) used for spatial smoothing in MVDR with FBSS. These results are shown in Fig. 9. While the three major arrivals at approximately 80.4°, 86.0°, and 100.6° seen in Fig. 8(a) continue to be identified in Fig. 9(a)–(d), there are some variations in both the DOAs and power levels of these arrivals between the blocks [in particular, the arrival at approximately 100.6° drops significantly in level in Fig. 9(b)]. In addition, a few fluctuating lower level arrivals are identified with the persistent arrival at approximately 92.8° being consistent with the arrival seen in Fig. 8(a). Fluctuations in the arrival levels evident in both Figs. 8 and 9 are a natural consequence of the time-evolving propagation conditions in this coastal shallow-water waveguide and the con-

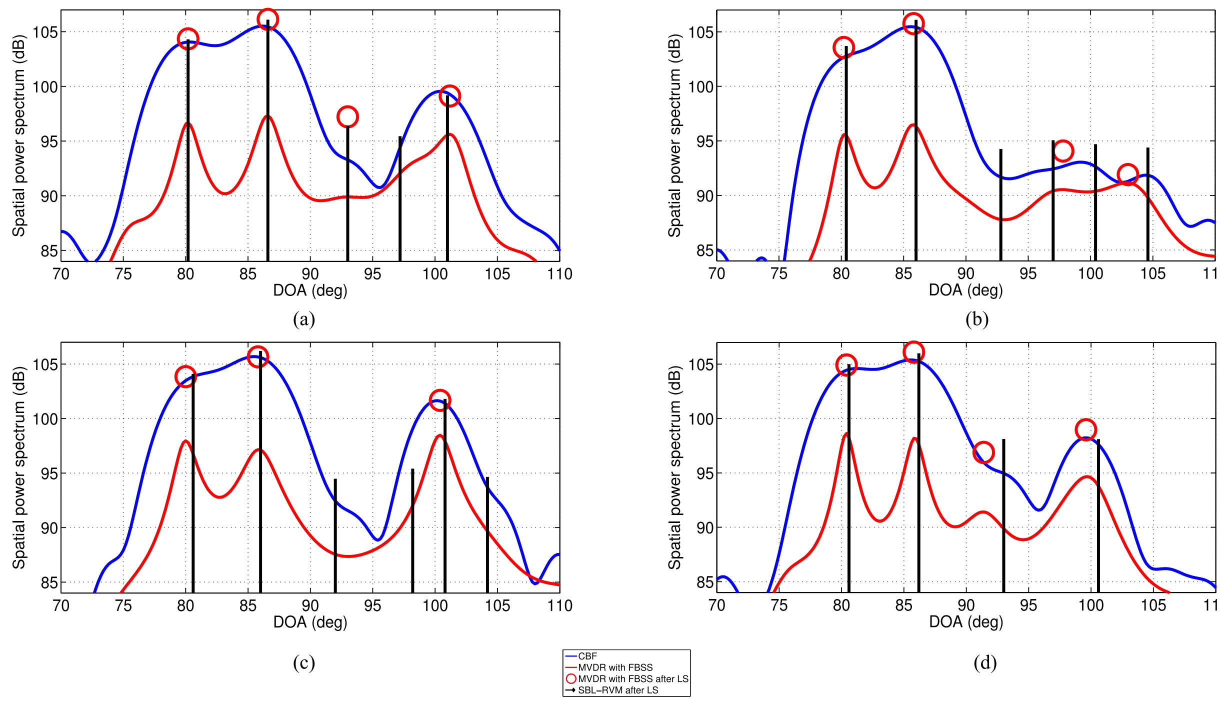

Fig. 9. Resolving multipath signals for the 1.9-kHz frequency in the HF97 experiment for the first 200 snapshots in blocks of 50 snapshots. Panels (a), (b), (c), and (d) correspond to the first, second, third, and fourth blocks of 50 snapshots ($\sim$4.25 s each), respectively.

structive/destructive interference between closely spaced (unresolved) multipath arrivals. Fig. 8(a) is representative of the persistent arrival structure seen across all four blocks in Fig. 9(a)–(d).

In Fig. 9(a)–(c), we note that MVDR with FBSS is not able to resolve the DOAs of all the coherent multipath signals due to reduced resolution in contrast to SBL-RVM. In all four panels in Fig. 9, SBL-RVM consistently estimated a DOA at approximately 92.8° which is consistent with the CBF spatial spectrum, but MVDR with FBSS is not able to identify this multipath in Fig. 9(b)–(c). Moreover, SBL-RVM estimated another DOA at approximately 97.0° in Fig. 9(a)–(c). This multipath is identified by MVDR with FBSS and CBF in Fig. 9(b), but they fail to identify this multipath in Fig. 9(a) and (c) due to its relatively low power level in these blocks compared to the 100.6° arrival and their poor resolution. Similarly, another arrival is estimated at approximately 104.6° by SBL-RVM in Fig. 9(b) and (c) while this is identified by MVDR with FBSS and CBF only in Fig. 9(b). These results demonstrate the superior performance of SBL-RVM with a small number of snapshots as compared to MVDR with FBSS.

VI. Conclusion

CS directly processed the signal from an array of sensors without first estimating the sensor covariance matrix and thus its performance did not deteriorate when resolving DOAs and power levels of coherent multipath signals in contrast to the MVDR beamformer. Though spatial smoothing helped in decorrelating the multipath signals, the MVDR processor lost resolution due to a reduction in effective aperture.

Empirical results of bias and variance showed that the performance of CS is comparable to the MVDR processor with spatial smoothing and sometimes outperforms the MVDR processor with spatial smoothing, giving better estimates of both the DOAs and the power levels with higher resolution and can be extremely useful for resolving multipath signals.

Finally, the successful application of CS in resolving multipath signals in the HF97 ocean acoustic experiment was demonstrated. CS resolved the DOAs of the multipath signals with higher resolution than MVDR with spatial smoothing and yields consistent results with the nonadaptive CBF.

References

[1] D. L. Donoho, "Compressed sensing," *IEEE Trans. Inf. Theory*, vol. 52, no. 4, pp. 1289–1306, Apr. 2006.

[2] D. L. Donoho, M. Elad, and V. N. Temlyakov, "Stable recovery of sparse overcomplete representations in the presence of noise," *IEEE Trans. Inf. Theory*, vol. 52, no. 1, pp. 6–18, Jan. 2006.

[3] E. J. Candes and T. Tao, "Decoding by linear programming," *IEEE Trans. Inf. Theory*, vol. 51, no. 12, pp. 4203–4215, Dec. 2005.

[4] E. J. Candes, J. Romberg, and T. Tao, "Robust uncertainty principles: Exact signal reconstruction from highly incomplete frequency information," *IEEE Trans. Inf. Theory*, vol. 52, no. 2, pp. 489–509, Feb. 2006.

[5] S. G. Lingala and M. Jacob, "Blind compressive sensing dynamic MRI," *IEEE Trans. Med. Imaging*, vol. 32, no. 6, pp. 1132–1145, Jun. 2013.

[6] J. Trzasko and A. Manduca, "Highly undersampled magnetic resonance image reconstruction via homotopic l_0-minimization," *IEEE Trans. Med. Imaging*, vol. 28, no. 1, pp. 106–121, Jan. 2009.

[7] C. R. Berger, S. Zhou, J. C. Preisig, and P. Willett, "Sparse channel estimation for multicarrier underwater acoustic communication: From subspace methods to compressed sensing," *IEEE Trans. Signal Process.*, vol. 58, no. 3, pp. 1708–1721, Mar. 2010.

[8] S. F. Cotter and B. D. Rao, "Sparse channel estimation via matching pursuit with application to equalization," *IEEE Trans. Commun.*, vol. 50, no. 3, pp. 374–377, Mar. 2002.

[9] M. A. Herman and T. Strohmer, "High-resolution radar via compressed sensing," *IEEE Trans. Signal Process.*, vol. 57, no. 6, pp. 2275–2284, Jun. 2009.

[10] M. Leigsnering, F. Ahmad, M. G. Amin, and A. M. Zoubir, "Compressive sensing based specular multipath exploitation for through-the-wall radar imaging," in *Proc. IEEE Int. Conf. Acoust. Speech Signal Process.*, May 2013, pp. 6004–6008.

[11] M. Aharon, M. Elad, and A. Bruckstein, "K -SVD: An algorithm for designing overcomplete dictionaries for sparse representation," *IEEE Trans. Signal Process.*, vol. 54, no. 11, pp. 4311–4322, Nov. 2006.

[12] J. L. Starck, M. Elad, and D. L. Donoho, "Image decomposition via the combination of sparse representations and a variational approach," *IEEE Trans. Image Process.*, vol. 14, no. 10, pp. 1570–1582, Oct. 2005.

[13] G. N. Lilis, D. Angelosante, and G. B. Giannakis, "Sound field reproduction using the Lasso," *IEEE/ACM Trans. Audio Speech Lang. Process.*, vol. 18, no. 8, pp. 1902–1912, Nov. 2010.

[14] A. Griffin, T. Hirvonen, C. Tzagkarakis, A. Mouchtaris, and P. Tsakalides, "Single-channel and multi-channel sinusoidal audio coding using compressed sensing," *IEEE/ACM Trans. Audio Speech Lang. Process.*, vol. 19, no. 5, pp. 1382–1395, Jul. 2011.

[15] A. Gholami and M. D. Sacchi, "A fast and automatic sparse deconvolution in the presence of outliers," *IEEE Trans. Geosci. Remote Sens.*, vol. 50, no. 10, pp. 4105–4116, Oct. 2012.

[16] X. X. Zhu and R. Bamler, "Super-resolution power and robustness of compressive sensing for spectral estimation with application to spaceborne tomographic SAR," *IEEE Trans. Geosci. Remote Sens.*, vol. 50, no. 1, pp. 247–258, Jan. 2012.

[17] J. Ma and F. X. L. Dimet, "Deblurring from highly incomplete measurements for remote sensing," *IEEE Trans. Geosci. Remote Sens.*, vol. 47, no. 3, pp. 792–802, Mar. 2009.

[18] C. Liu, Y. V. Zakharov, and T. Chen, "Broadband underwater localization of multiple sources using basis pursuit de-noising," *IEEE Trans. Signal Process.*, vol. 60, no. 4, pp. 1708–1717, Apr. 2012.

[19] M. Nagahara, D. E. Quevedo, and J. Ostergaard, "Sparse packetized predictive control for networked control over erasure channels," *IEEE Trans. Autom. Control*, vol. 59, no. 7, pp. 1899–1905, Jul. 2014.

[20] J. Wright, A. Y. Yang, A. Ganesh, S. S. Sastry, and Y. Ma, "Robust face recognition via sparse representation," *IEEE Trans. Pattern Anal. Mach. Intell.*, vol. 31, no. 2, pp. 210–227, Feb. 2009.

[21] X. Mei and H. Ling, "Robust visual tracking and vehicle classification via sparse representation," *IEEE Trans. Pattern Anal. Mach. Intell.*, vol. 33, no. 11, pp. 2259–2272, Nov. 2011.

[22] S. G. Mallat and Z. Zhang, "Matching pursuits with time-frequency dictionaries," *IEEE Trans. Signal Process.*, vol. 41, no. 12, pp. 3397–3415, Dec. 1993.

[23] J. A. Tropp and A. C. Gilbert, "Signal recovery from random measurements via orthogonal matching pursuit," *IEEE Trans. Inf. Theory*, vol. 53, no. 12, pp. 4655–4666, Dec. 2007.

[24] D. Needell and R. Vershynin, "Signal recovery from incomplete and inaccurate measurements via regularized orthogonal matching pursuit," *IEEE J. Sel. Topics Signal Process.*, vol. 4, no. 2, pp. 310–316, Apr. 2010.

[25] S. Chen, D. Donoho, and M. Saunders, "Atomic decomposition by basis pursuit," *SIAM J. Sci. Comput.*, vol. 20, no. 1, pp. 33–61, 1998.

[26] A. Xenaki, P. Gerstoft, and K. Mosegaard, "Compressive beamforming," *J. Acoust. Soc. Amer.*, vol. 136, no. 1, pp. 260–271, 2014.

[27] E. J. Candes, M. B. Wakin, and S. P. Boyd, "Enhancing sparsity by reweighted l_1 minimization," *J. Fourier Anal. Appl.*, vol. 14, no. 5–6, pp. 877–905, 2008.

[28] I. F. Gorodnitsky and B. D. Rao, "Sparse signal reconstruction from limited data using FOCUSS: A reweighted minimum norm algorithm," *IEEE Trans. Signal Process.*, vol. 45, no. 3, pp. 600–616, Mar. 1997.

[29] R. Chartrand and W. Yin, "Iteratively reweighted algorithms for compressive sensing," in *Proc. IEEE Int. Conf. Acoust. Speech Signal Process.*, Mar. 2008, pp. 3869–3872.

[30] M. E. Tipping, "Sparse Bayesian learning and the relevance vector machine," *J. Mach. Learn. Res.*, vol. 1, pp. 211–244, Sep. 2001.

[31] S. D. Babacan, R. Molina, and A. K. Katsaggelos, "Bayesian compressive sensing using Laplace priors," *IEEE Trans. Image Process.*, vol. 19, no. 1, pp. 53–63, Jan. 2010.

[32] M. A. T. Figueiredo, "Adaptive sparseness for supervised learning," *IEEE Trans. Pattern Anal. Mach. Intell.*, vol. 25, no. 9, pp. 1150–1159, Sep. 2003.

[33] M. W. Seeger, "Bayesian inference and optimal design for the sparse linear model," *J. Mach. Learn. Res.*, vol. 9, pp. 759–813, Jun. 2008.

[34] J. A. Tropp, A. C. Gilbert, and M. J. Strauss, "Algorithms for simultaneous sparse approximation. Part I: Greedy pursuit," *Signal Process.*, vol. 86, no. 3, pp. 572–588, 2006.

[35] S. F. Cotter, B. D. Rao, K. Engan, and K. Kreutz-Delgado, "Sparse solutions to linear inverse problems with multiple measurement vectors," *IEEE Trans. Signal Process.*, vol. 53, no. 7, pp. 2477–2488, Jul. 2005.

[36] J. Chen and X. Huo, "Theoretical results on sparse representations of multiple-measurement vectors," *IEEE Trans. Signal Process.*, vol. 54, no. 12, pp. 4634–4643, Dec. 2006.

[37] J. A. Tropp, "Algorithms for simultaneous sparse approximation. Part II: Convex relaxation," *Signal Process.*, vol. 86, no. 3, pp. 589–602, 2006.

[38] M. H. Wei, W. R. Scott, and J. H. McClellan, "Jointly sparse vector recovery via reweighted l_1 minimization," in *Proc. IEEE Int. Conf. Acoust. Speech Signal Process*, Mar. 2012, pp. 3929–3932.

[39] D. P. Wipf and B. D. Rao, "An empirical Bayesian strategy for solving the simultaneous sparse approximation problem," *IEEE Trans. Signal Process.*, vol. 55, no. 7, pp. 3704–3716, Jul. 2007.

[40] M. Carlin, P. Rocca, G. Oliveri, F. Viani, and A. Massa, "Directions-of-arrival estimation through bayesian compressive sensing strategies," *IEEE Trans. Antennas Propag.*, vol. 61, no. 7, pp. 3828–3838, Jul. 2013.

[41] D. Malioutov, M. Cetin, and A. S. Willsky, "A sparse signal reconstruction perspective for source localization with sensor arrays," *IEEE Trans. Signal Process.*, vol. 53, no. 8, pp. 3010–3022, Aug. 2005.

[42] M. M. Hyder and K. Mahata, "Direction-of-arrival estimation using a mixed $l_{2,0}$ norm approximation," *IEEE Trans. Signal Process.*, vol. 58, no. 9, pp. 4646–4655, Sep. 2010.

[43] Z. Tan and A. Nehorai, "Sparse direction of arrival estimation using coprime arrays with off-grid targets," *IEEE Signal Process. Lett.*, vol. 21, no. 1, pp. 26–29, 2014.

[44] X. Wei, Y. Yuan, and Q. Ling, "DOA estimation using a greedy block coordinate descent algorithm," *IEEE Trans. Signal Process.*, vol. 60, no. 12, pp. 6382–6394, 2012.

[45] S. Haykin, J. H. Justice, N. L. Owsley, J. L. Yen, and A. C. Kak, *Array Signal Processing*, Englewood Cliffs, NJ, USA: Prentice-Hall, 1985.

[46] A. K. Luthra, "A solution to the adaptive nulling problem with a look-direction constraint in the presence of coherent jammers," *IEEE Trans. Antennas Propag.*, vol. 34, no. 5, pp. 702–710, May 1986.

[47] P. Zetterberg and B. Ottersten, "The spectrum efficiency of a base station antenna array system for spatially selective transmission," *IEEE Trans. Veh. Technol.*, vol. 44, no. 3, pp. 651–660, Aug. 1995.

[48] J. H. Winters, "On the capacity of radio communication systems with diversity in a Rayleigh fading environment," *IEEE J. Sel. Areas Commun.*, vol. 5, no. 5, pp. 871–878, Jun. 1987.

[49] H. L. Van Trees, *Detection, Estimation, and Modulation Theory, Optimum Array Processing*, New York, NY, USA: Wiley, 2004.

[50] J. E. Evans, J. R. Johnson, and D. F. Sun, "Application of advanced signal processing techniques to angle of arrival estimation in A.T.C. Navigation and Surveillance Systems," Lexington, MA, USA, Tech. Rep. 582, MIT Lincoln Lab., 1982.

[51] S. U. Pillai and B. H. Kwon, "Forward/backward spatial smoothing techniques for coherent signal identification," *IEEE Trans. Acoust. Speech Signal Process.*, vol. 37, no. 1, pp. 8–15, Jan. 1989.

[52] R. T. Williams, S. Prasad, A. K. Mahalanabis, and L. H. Sibul, "An improved spatial smoothing technique for bearing estimation in a multipath environment," *IEEE Trans. Acoust. Speech Signal Process.*, vol. 36, no. 4, pp. 425–432, Apr. 1988.

[53] D. Wipf and B. Rao, "Sparse Bayesian learning for basis selection," *IEEE Trans. Signal Process.*, vol. 52, no. 8, pp. 2153–2164, Aug. 2004.

[54] S. M. Kay, *Fundamentals of Statistical Signal Processing: Estimation Theory*, Englewood Cliffs, NJ, USA: Prentice-Hall, 1993, Ch. 15.

[55] S. Fortunati, R. Grasso, F. Gini, and M. S. Greco, "Single snapshot DOA estimation using compressed sensing," in *Proc. IEEE Int. Conf. Acoust. Speech Signal Process.*, May 2014, pp. 2297–2301.

[56] I. Bilik, "Spatial compressive sensing for direction-of-arrival estimation of multiple sources using dynamic sensor arrays," *IEEE Trans. Aerosp. Electron. Syst.*, vol. 47, no. 3, pp. 1754–1769, Jul. 2011.

[57] X. Li, X. Ma, S. Yan, and C. Hou, "Single snapshot DOA estimation by compressive sampling," *Appl. Acoust.*, vol. 74, no. 7, pp. 926–930, 2013.

[58] R. Ward, "Compressed sensing with cross validation," *IEEE Trans. Inf. Theory*, vol. 55, no. 12, pp. 5773–5782, Dec. 2009.

[59] R. Tibshirani, "Regression shrinkage and selection via the Lasso," *J. R. Stat. Soc. Ser. B, Stat. Methodol.*, vol. 58, no. 1, 1996, pp. 267–288.

[60] P. Boufounos, M. F. Duarte, and R. G. Baraniuk, "Sparse signal reconstruction from noisy compressive measurements using cross validation," in *Proc. IEEE Workshop Stat. Signal Process.*, Aug. 2007, pp. 299–303.

[61] L. He and L. Carin, "Exploiting structure in wavelet-based Bayesian compressive sensing," *IEEE Trans. Signal Process.*, vol. 57, no. 9, pp. 3488–3497, Sep. 2009.

[62] Y. Huang *et al.*, "Bayesian nonparametric dictionary learning for compressed sensing MRI," *IEEE Trans. Image Process.*, vol. 23, no. 12, pp. 5007–5019, Dec. 2014.

[63] D. J. C. MacKay, "Bayesian interpolation," *Neural Comput.*, vol. 4, no. 3, pp. 415–447, May 1992.
[64] Z. Zhang, T. P. Jung, S. Makeig, Z. Pi, and B. D. Rao, "Spatiotemporal sparse Bayesian learning with applications to compressed sensing of multichannel physiological signals," *IEEE Trans. Neural Syst. Rehabil. Eng.*, vol. 22, no. 6, pp. 1186–1197, Nov. 2014.
[65] L. Du, T. Yardibi, J. Li, and P. Stoica, "Review of user parameter-free robust adaptive beamforming algorithms," *Digital Signal Process.*, vol. 19, no. 4, pp. 567–582, 2009.
[66] C. D. Richmond, "Capon algorithm mean-squared error threshold SNR prediction and probability of resolution," *IEEE Trans. Signal Process.*, vol. 53, no. 8, pp. 2748–2764, Aug. 2005.
[67] Q. T. Zhang, "Probability of resolution of the MUSIC algorithm," *IEEE Trans. Signal Process.*, vol. 43, no. 4, pp. 978–987, Apr. 1995.
[68] M. A. Herman and T. Strohmer, "General deviants: An analysis of perturbations in compressed sensing," *IEEE J. Sel. Top. Signal Process.*, vol. 4, no. 2, pp. 342–349, Apr. 2010.
[69] Y. Chi, L. L. Scharf, A. Pezeshki, and A. R. Calderbank, "Sensitivity to basis mismatch in compressed sensing," *IEEE Trans. Signal Process.*, vol. 59, no. 5, pp. 2182–2195, May 2011.
[70] P. Stoica and P. Babu, "Sparse estimation of spectral lines: Grid selection problems and their solutions," *IEEE Trans. Signal Process.*, vol. 60, no. 2, pp. 962–967, Feb. 2012.
[71] E. T. Northardt, I. Bilik, and Y. I. Abramovich, "Spatial compressive sensing for direction-of-arrival estimation with bias mitigation via expected likelihood," *IEEE Trans. Signal Process.*, vol. 61, no. 5, pp. 1183–1195, Mar. 2013.
[72] G. Tang, B. N. Bhaskar, P. Shah, and B. Recht, "Compressed sensing off the grid," *IEEE Trans. Inf. Theory*, vol. 59, no. 11, pp. 7465–7490, Nov. 2013.
[73] Z. Yang, L. Xie, and C. Zhang, "Off-grid direction of arrival estimation using sparse Bayesian inference," *IEEE Trans. Signal Process.*, vol. 61, no. 1, pp. 38–43, Jan. 2013.
[74] M. E. Tipping, "Bayesian inference: An introduction to principles and practice in machine learning," *Advanced Lectures on Machine Learning*, Berlin, Germany: Springer-Verlag, 2004, pp. 41–62.
[75] M. A. T. Figueiredo, R. D. Nowak, and S. J. Wright, "Gradient projection for sparse reconstruction: Application to compressed sensing and other inverse problems," *IEEE J. Sel. Top. Signal Process.*, vol. 1, no. 4, pp. 586–597, Dec. 2007.
[76] C. F. Mecklenbrauker, P. Gerstoft, A. Panahi, and M. Viberg, "Sequential Bayesian sparse signal reconstruction using array data," *IEEE Trans. Signal Process.*, vol. 61, no. 24, pp. 6344–6354, Dec. 2013.
[77] B. D. Rao, K. Engan, S. F. Cotter, J. Palmer, and K. Kreutz-Delgado, "Subset selection in noise based on diversity measure minimization," *IEEE Trans. Signal Process.*, vol. 51, no. 3, pp. 760–770, Mar. 2003.
[78] P. Stoica and A. Nehorai, "Music, maximum likelihood, and Cramer-Rao bound," *IEEE Trans. Acoust. Speech Signal Process.*, vol. 37, no. 5, pp. 720–741, May 1989.
[79] N. M. Carbone and W. S. Hodgkiss, "Effects of tidally driven temperature fluctuations on shallow-water acoustic communications at 18 kHz," *IEEE J. Ocean. Eng.*, vol. 25, no. 1, pp. 84–94, Jan. 2000.
[80] W. S. Hodgkiss, W. A. Kuperman, and D. E. Ensberg, "Channel impulse response fluctuations at 6 kHz in shallow water," *Impact of Littoral Environmental Variability of Acoustic Predictions and Sonar Performance*, New York, NY, USA: Springer-Verlag, 2002, pp 295–302.

Anup Das was born in Bhubaneswar, Orissa state, India, on May 15, 1991. He received the B.Tech. degree in electronics and communication engineering from the Indian Institute of Technology (IIT), Guwahati, India, in 2013 and the M.S. degree in electrical engineering (signal and image processing) from the University of California, San Diego, La Jolla, CA, USA, in 2015, where he is currently working toward the Ph.D. degree in electrical engineering (signal and image processing).

His research interests are in the general areas of statistical signal processing, sparse signal processing, and machine learning and Bayesian inference with applications to array signal processing and biomedical signal processing.

Mr. Das received the University of California, San Diego Electrical and Computer Engineering (ECE) Departmental Fellowship in 2013.

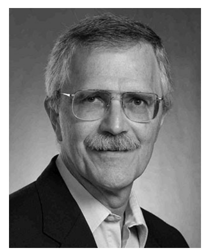

William S. Hodgkiss (S'68–M'75) received the Ph.D. degree in electrical engineering from Duke University, Durham, NC, USA, in 1975.

Since 1978, he has been a member of the faculty of the Scripps Institution of Oceanography, University of California, San Diego (UCSD), La Jolla, CA, USA and on the staff of the Marine Physical Laboratory where currently he is Deputy Director. He also has a joint appointment with the Department of Electrical and Computer Engineering in the Jacobs School of Engineering. During 1998–2002, he served as Deputy Director—Scientific Affairs at Scripps and Associate Vice Chancellor—Marine Sciences. Currently he serves as Senior Associate Vice Chancellor for Academic Planning and Resources at UCSD. His present research interests are in the areas of signal processing, communications, wireless sensor networks, propagation modeling, ambient noise, and environmental inversions, with applications of these to underwater acoustics and electromagnetic wave propagation.

Dr. Hodgkiss is a Fellow of the Acoustical Society of America.

Peter Gerstoft (M'13) received the Ph.D. from the Technical University of Denmark, Lyngby, Denmark, in 1986.

From 1987 to 1992, he was with Ødegaard and Danneskiold-Samsøe, Copenhagen, Denmark. From 1992 to 1997, he was at Nato Undersea Research Centre, La Spezia, Italy. Since 1997, he has been with the Marine Physical Laboratory, University of California, San Diego (UCSD), La Jolla, CA, USA. His research interests include modeling and inversion of acoustic, elastic, and electromagnetic signals.

Dr. Gerstoft is a Fellow of Acoustical Society of America and an elected member of the International Union of Radio Science, Commission F.